Editors' Suggestion

# Universal Anomalous Diffusion of Quantized Vortices in Ultraquantum Turbulence

Satoshi Yui,[1,2,*] Yuan Tang,[3,4,*] Wei Guo,[3,4,†] Hiromichi Kobayashi,[5,6,‡] and Makoto Tsubota[1,2,§]

[1]Department of Physics, Osaka Metropolitan University, 3-3-138 Sugimoto, Sumiyoshi-ku, Osaka 558-8585, Japan
[2]Nambu Yoichiro Institute of Theoretical and Experimental Physics (NITEP), Osaka Metropolitan University, Osaka 558-8585, Japan
[3]National High Magnetic Field Laboratory, 1800 East Paul Dirac Drive, Tallahassee, Florida 32310, USA
[4]Mechanical Engineering Department, FAMU-FSU College of Engineering, Florida State University, Tallahassee, Florida 32310, USA
[5]Research and Education Center for Natural Sciences, Keio University, 4-1-1 Hiyoshi, Kohoku-ku, Yokohama 223-8521, Japan
[6]Department of Physics, Keio University, 4-1-1 Hiyoshi, Kohoku-ku, Yokohama 223-8521, Japan

(Received 26 February 2022; revised 29 April 2022; accepted 9 June 2022; published 5 July 2022)

In classical viscous fluids, turbulent eddies are known to be responsible for the rapid spreading of embedded particles. However, in inviscid quantum fluids where the turbulence is induced by a chaotic tangle of quantized vortices, dispersion of the particles can be achieved via a nonclassical mechanism, i.e., their binding to the evolving vortices. However, knowledge on how the vortices diffuse and spread in quantum-fluid turbulence is very limited, especially for the so-called ultraquantum turbulence (UQT) generated by a random tangle of vortices. Here we report a systematic numerical study of the apparent diffusion of vortices in UQT in superfluid helium-4 using the full Biot-Savart simulation. We reveal that the vortices in the superfluid exhibit a universal anomalous diffusion (superdiffusion) at small times, which transits to normal diffusion at large times. This behavior is found to be the result of a generic scaling property of the vortex velocity. Our simulation at finite temperatures also nicely reproduces recent experimental observations. The knowledge obtained from this study may form the base for understanding turbulent transport and universal vortex dynamics in various quantum fluids.

DOI: 10.1103/PhysRevLett.129.025301

Turbulent diffusion in classical fluids has been studied extensively due to its wide range of applications such as chemical mixing in star formation [1] and airborne virus transmission [2]. It has been known that the turbulent eddies can carry embedded particles, leading to some well-known time scaling of the particle separation, such as Richardson's $t^3$ law [3]. However, this knowledge does not apply to inviscid quantum fluids such as superfluid helium-4 (He II) and atomic Bose-Einstein condensates (BECs), since the injected particles are not entrained by the superfluid flow at low temperatures. Instead, a distinct transport mechanism exists, i.e., binding to the evolving quantized vortices.

In a quantum fluid, turbulence can be induced by a chaotic tangle of quantized vortex lines [4], which are line-shaped topological defects featured by a circulating flow with a quantized circulation $\kappa = h/m$, where $h$ is Planck's constant and $m$ is the mass of the bosons constituting the superfluid [5]. The vortices evolve with time chaotically, and they also undergo reconnections when they move across each other [6]. Depending on the internal structure of the vortex tangle, two forms of turbulent flows may emerge in a quantum fluid [7,8]. The first form is called quasiclassical turbulence, where the vortices in the tangle can polarize locally and form bundles to mimic classical vortices [9]. In this case, the induced velocity field can exhibit various classical features at length scales greater than the mean vortex-line spacing $\ell$ [10,11]. On the other hand, when the vortices in the tangle arrange themselves randomly, an ultraquantum turbulence (UQT) with no classical analog is generated, where the flow field fluctuates at scales comparable to $\ell$ without any large-scale motion [12]. Particles in a quantum fluid can bind to the vortex cores and subsequently move together with the vortices [13–16]. Knowing how vortices diffuse in space is therefore crucial for understanding turbulent transport in quantum fluids.

So far, there have been very limited studies on the apparent diffusion of vortices in quantum-fluid turbulence. On the theoretical side, the overall expansion of a decaying random vortex tangle near a solid wall [17] and in bulk He II [18] was simulated. However, these studies only provide limited insights into the diffusion behavior of vortices in a fully developed turbulence. In a recent experiment, Tang *et al.* [19] decorated the vortices in UQT generated by counterflow in He II with solidified deuterium tracer particles. They observed that the vortices undergo anomalous diffusion (superdiffusion) at small times. Their measured diffusion time exponent appears to be insensitive to both the temperature and the vortex-line density, suggesting a possible generic nature of this vortex-diffusion behavior. However, since the experiment was conducted in a narrow temperature range (i.e., 1.7–2.0 K), a reliable conclusion cannot be achieved.

 

In this Letter, we report a systematic numerical study of the apparent diffusion of individual vortices in UQT in He II using the full Biot-Savart simulation [20]. We reveal that in pure superfluid the vortices in UQT indeed undergo superdiffusion at small times with a *universal* diffusion exponent regardless how dense the tangle is. At large times, the superdiffusion transits to normal diffusion due to vortex reconnections. Our analysis shows that this universal diffusion behavior is caused by a generic temporal correlation of the vortex velocity, which should exist in other quantum fluids where the Biot-Savart law applies. At finite temperatures, the viscous effect is found to only mildly affect the vortex diffusion, which nicely explains the experimental observations. Since UQT can be produced by counterflow in quantum two-fluid systems such as He II [21,22], atomic BECs [23], and superfluid neutron stars [24,25], and it can also spontaneously emerge following a second-order phase transition in quantum fluids via the Kibble-Zurek mechanism [26,27], the knowledge obtained in our study may also offer valuable insights into the evolution and quenching dynamics of these diverse quantum fluids.

*Vortex diffusion in a pure superfluid.*—Like many other quantum fluids, He II can be considered as a mixture of two miscible fluid components, i.e., an inviscid superfluid and a viscous normal fluid (i.e., collection of thermal quasiparticles) [28]. The normal-fluid fraction in He II drops with decreasing the temperature and becomes negligible below 1 K. Experimentally, an UQT can be produced in He II at zero-temperature limit by injecting small vortex rings [12]. Here, we adopt a similar method numerically to study vortex diffusion in UQT in pure superfluid. As shown in Fig. 1(a), we first place 64 randomly oriented vortex rings (radius, $R_{\rm in} = 0.11$ mm) in a cubical computational box (side length, $D = 1$ mm) with periodic boundary conditions in all three axial directions. These vortices are described by the vortex-filament model [29], and each vortex filament is discretized into a series of points. In the absence of the normal fluid, a vortex-filament point at $\mathbf{s}$ moves at the local superfluid velocity $\mathbf{v}_s(\mathbf{s})$ as given by the Biot-Savart law [29,30],

$$\frac{d\mathbf{s}}{dt} = \mathbf{v}_s(\mathbf{s}) = \frac{\kappa}{4\pi}\int \frac{(\mathbf{s}_1 - \mathbf{s}) \times d\mathbf{s}_1}{|\mathbf{s}_1 - \mathbf{s}|^3}. \tag{1}$$

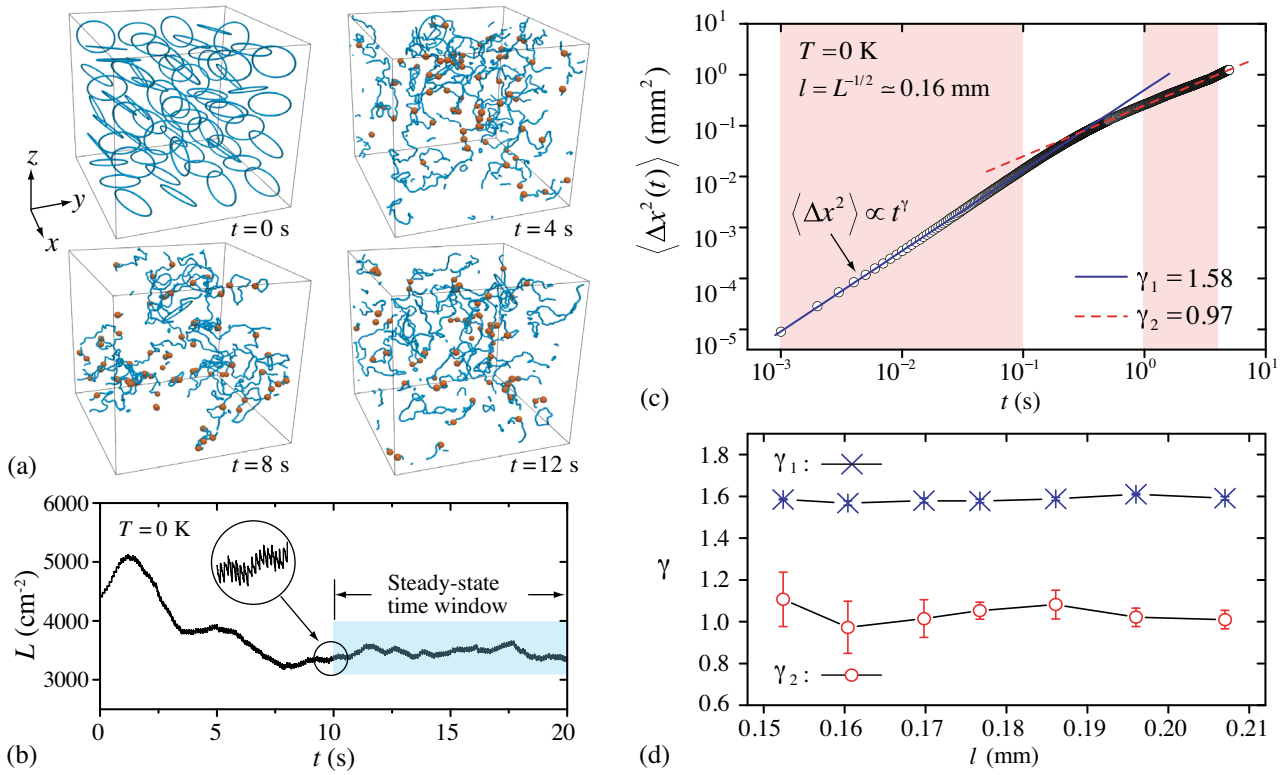


FIG. 1. (a) Snapshots of an evolving random vortex tangle. The red dots represent the vortex-filament points tracked for diffusion analysis. (b) Variation of the corresponding vortex-line density $L(t)$. The enlargement in the inset shows fluctuations in $L$ due to ring injections. (c) Mean-square displacement of the vortices $\langle \Delta x^2(t) \rangle$ in the $x$ direction. The solid and dashed lines are power-law fits to the data in the shaded regions. (d) Diffusion exponents $\gamma$ averaged over $x$, $y$, and $z$ directions versus the mean vortex-line spacing $\ell = L^{-1/2}$. The error bars (barely visible for $\gamma_1$) represent the standard deviations of the $\gamma$ values for diffusion in the three axial directions.

The time evolution of the vortices can be obtained through a temporal integration of Eq. (1) (see details and videos in the Supplemental Material [31], which includes Refs. [32–34]). When two vortex filaments approach to have a minimum separation less than 0.008 mm, we reconnect them at the location of the minimum separation following the procedures as detailed in Refs. [30,35]. We also inject a randomly oriented vortex ring of radius $R_{\rm in}$ at a random location in the computational box with a repetition time $t_{\rm in}$ to balance the cascade loss of the vortices [30]. Figure 1(a) shows the evolution of the vortex tangle with $t_{\rm in} = 0.08$ s. The variation of the vortex-line density $L$ (i.e., vortex length per unit volume) is shown in Fig. 1(b). After about 10 s, $L$ settles to a nearly constant level. This steady-state $L$ level can be tuned by varying $t_{\rm in}$.

To study vortex diffusion, we track randomly chosen vortex-filament points and analyze their mean-square displacement (MSD) along each axis (see Supplemental Material [31]). Figure 1(c) shows the MSD of the vortices in the $x$ direction $\langle \Delta x^2(t)\rangle = \langle [x(t_0+t) - x(t_0)]^2\rangle$ in a representative case, where $t_0$ is the reference time when a vortex-filament point is tracked and the angle brackets denote an ensemble average of all the tracked points in the steady state. Usually, a power-law scaling $\langle \Delta x^2(t)\rangle \propto t^{\gamma}$ is expected, where the exponent $\gamma$ defines different diffusion regimes, i.e., normal diffusion ($\gamma = 1$) and anomalous diffusion (superdiffusion at $\gamma > 1$ and subdiffusion at $\gamma < 1$) [36]. Our data exhibit a clear superdiffusion regime ($\gamma_1 = 1.58$) at small $t$ and a normal diffusion regime ($\gamma_2 = 0.97$) at large $t$. Simulations conducted at other $L$ also show similar behaviors. The derived $\gamma_1$ and $\gamma_2$ are plotted in Fig. 1(d) as a function of the mean vortex-line spacing $\ell = L^{-1/2}$. It is clear that $\gamma_1$ is about 1.6 at all $\ell$ values. $\gamma_2$ is around 1, but has sizable variations in the three axial directions. These variations are caused by the reduced sample numbers at large $t$, as well as the limited size of the computational box (see Supplemental Material [31]).

*Explanation on vortex-diffusion scaling.*—Superdiffusion has been observed in various systems, such as hopping of cold atoms in an optical lattice [37] and cellular transport in biological systems [38]. For systems involving random walkers, the appearance of superdiffusion is usually attributed to Lévy flights, i.e., occasional long-distance hops of the walkers [39]. These flights lead to power-law tails of the walkers' displacement distribution $P(\Delta x) \propto |\Delta x|^{-\alpha}$, which is flat enough (i.e., $\alpha < 3$) to cause superdiffusion [40]. In He II, large displacements of the vortices over short times can occur at the locations of vortex reconnections [41]. However, we find that these reconnections always result in tails of the vortex displacement distribution $P(\Delta x)$ steeper than $|\Delta x|^{-3}$ (see Supplemental Material [31]). Therefore, they cannot account for the observed vortex superdiffusion. On the other hand, superdiffusion can emerge if the motion of the walkers is not completely random but has extended temporal correlations [40,42]. To see this, we write the MSD of a vortex-filament point $\langle \Delta x^2(t)\rangle$ in terms of its velocity $v_x(t)$ as [43]

$$\langle \Delta x^2(t)\rangle = 2\int_0^t dt_0 \int_0^{t-t_0} dt' \langle v_x(t_0) v_x(t_0+t')\rangle. \quad (2)$$

For a fully developed random tangle, the vortex-velocity temporal correlation function $C_x(t') = \langle v_x(t_0) v_x(t_0+t')\rangle$ only depends on the lapse time $t'$. If $C_x(t')$ shows a power-law scaling $C_x(t') \propto t'^{-\beta}$ over a large time interval, $\langle \Delta x^2(t)\rangle$ would scale as $\langle \Delta x^2(t)\rangle \propto t^{2-\beta}$ according to Eq. (2) and can exhibit superdiffusion when $\beta < 1$. In Fig. 2(a), we show the calculated $C_x(t')$ for a representative tangle with $\ell = 0.16$ mm. There is a clear power-law scaling with a fitted exponent $\beta = 0.42$, which leads to $\langle \Delta x^2(t)\rangle \propto t^{1.58}$, matching nicely the superdiffusion exponent reported in Fig. 1. Similar results are obtained for other cases at different $\ell$, which confirms that the universal vortex superdiffusion at small $t$ is caused by the temporal correlation of the vortex velocity. This correlation is an intrinsic feature of UQT.

The transition to the normal diffusion at large $t$ was also observed experimentally by Tang *et al.* [19]. They proposed that this transition is caused by vortex reconnections, which effectively randomize the motion of the participating

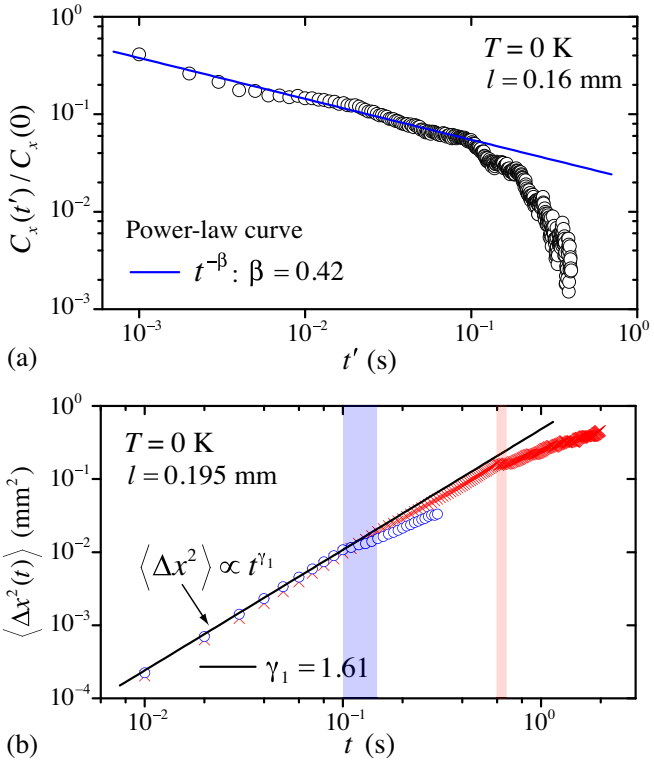


FIG. 2. (a) Vortex-velocity temporal correlation function $C_x(t')$ for a representative tangle exhibiting a power-law scaling that leads to the observed superdiffusion. (b) $\langle \Delta x^2(t)\rangle$ data for two selected groups of vortex-filament points (i.e., blue circles and red crosses), which encountered their first reconnection event in the diffusion time intervals shaded by the respective colors.

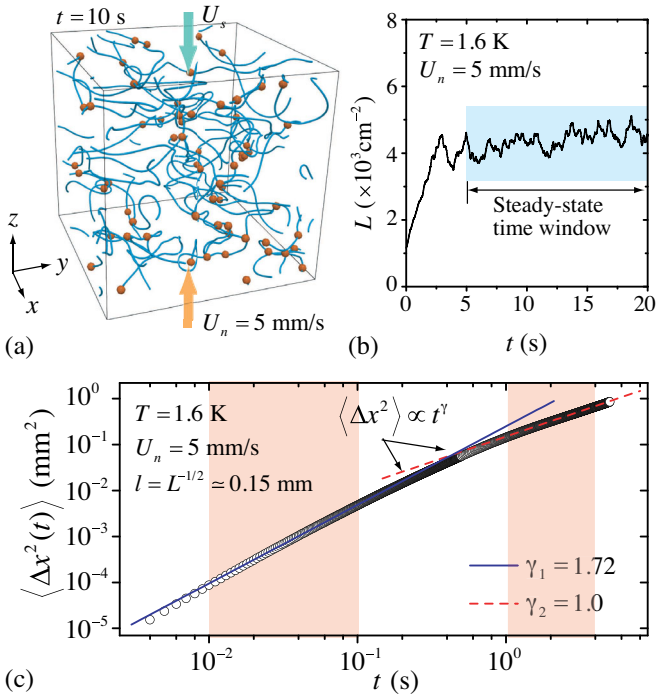


FIG. 3. (a) A representative snapshot of the vortex tangle produced by counterflow at $T = 1.6$ K with $U_n = 5$ mm/s. The red dots represent the tracked vortex-filament points. (b) Evolution of the vortex-line density $L(t)$. (c) Mean-square displacement of the vortices in the $x$ direction in counterflow. The solid and dashed lines are power-law fits to the data in the shaded regions.

vortex-filament points and hence suppress their velocity temporal correlation. To verify this view, we show the MSD of two selected groups of vortex-filament points for the case with $\ell = 0.195$ mm in Fig. 2(b). These two groups encountered their first reconnection event in the diffusion time interval $t = 0.1$–$0.15$ and $t = 0.6$–$0.65$ s, respectively. Obvious deviation from the superdiffusion scaling is observed for each group following the reconnection event, which clearly proves the causality between vortex reconnections and the transition toward the normal diffusion.

*Finite-temperature effect.*—At finite temperatures, the vortices experience a drag force as they move through the normal fluid due to scattering of the thermal quasiparticles in He II [44]. The velocity of a vortex-filament point at $\mathbf{s}$ is now given by [29,30]

$$d\mathbf{s}/dt = \mathbf{v}_s(\mathbf{s}) + \alpha\mathbf{s}' \times (\mathbf{v}_n - \mathbf{v}_s) - \alpha'\mathbf{s}' \times [\mathbf{s}' \times (\mathbf{v}_n - \mathbf{v}_s)], \tag{3}$$

where $\alpha$ and $\alpha'$ are temperature-dependent mutual friction coefficients [45], $\mathbf{s}'$ is the unit tangent vector along the filament, and $\mathbf{v}_n$ is the normal-fluid velocity. We then generate a steady-state vortex tangle using two distinct methods. The first method is the same as the one adopted at 0 K, i.e., by randomly injecting small vortex rings in the computational box with static normal fluid (i.e., $\mathbf{v}_n = 0$). The second method is via thermal counterflow as adopted in the experiment by Tang *et al.* [19].

In He II, a counterflow can be generated by an applied heat flux $q$, where the normal fluid moves in the heat flow direction at a mean velocity $U_n = q/\rho s T$, while the superfluid moves oppositely at $U_s = (\rho_n/\rho_s)U_n$ [28]. Here, $\rho = \rho_n + \rho_s$ is the total density, and $s$ is the He II specific entropy [46]. To compare with the experiment where the normal-fluid flow is laminar, we set $\mathbf{v}_n = U_n\hat{\mathbf{e}}_z$ and $\mathbf{v}_s$ as the sum of $-U_s\hat{\mathbf{e}}_z$ and the induced velocity given in Eq. (1). We then place a few randomly oriented seed vortex rings in the computational box. These rings can grow and reconnect, eventually leading to a fully developed tangle [20]. A snapshot of such a tangle at $T = 1.6$ K and $U_n = 5$ mm/s is shown in Fig. 3(a), and the line-density evolution is given in Fig. 3(b). In the steady-state time window (i.e., 5–20 s), we track randomly selected vortex-filament points and analyze their MSD in the directions perpendicular to the counterflow. Representative data for $\langle \Delta x^2(t) \rangle$ are shown in Fig. 3(c). Again, a superdiffusion regime is observed at small $t$, which transits to normal diffusion at large $t$.

In Figs. 4(a) and 4(b), we collect the derived superdiffusion exponent $\gamma_1$ for tangles generated, respectively,

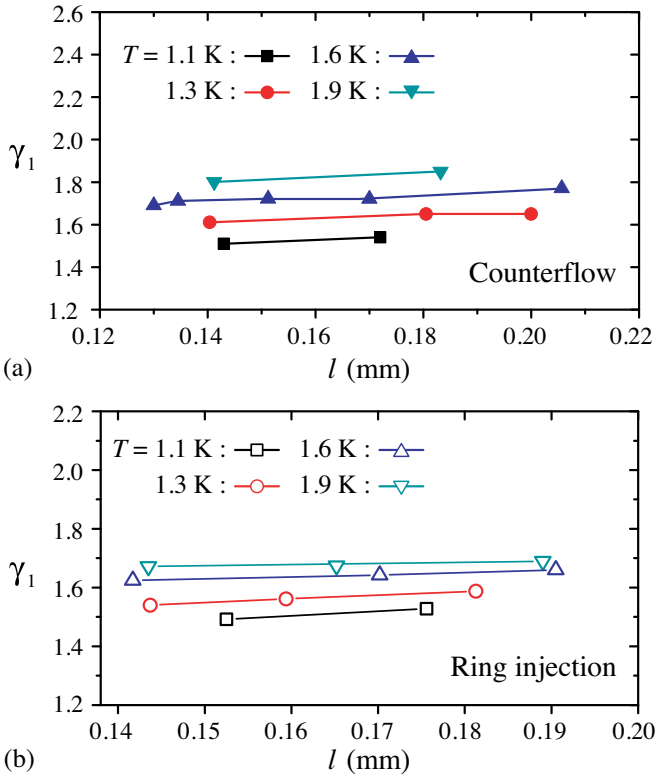


FIG. 4. (a) Diffusion exponent $\gamma_1$ versus $\ell$ for vortex tangles produced by counterflow at various $T$. (b) $\gamma_1$ versus $\ell$ for tangles produced by vortex-ring injection.

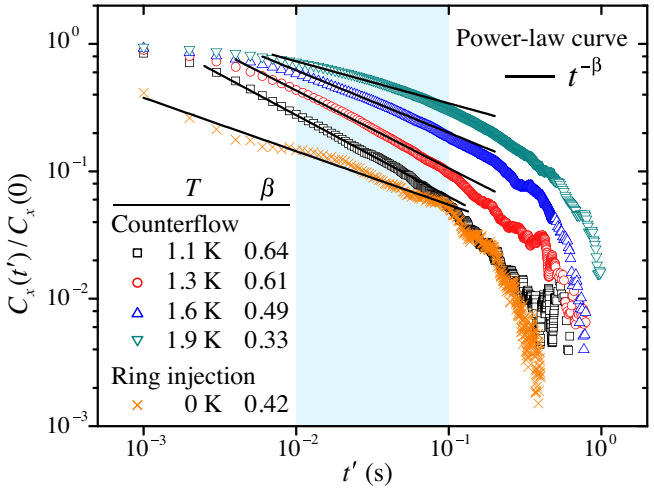


FIG. 5. Vortex-velocity temporal correlation function $C_x(t')$ at various $T$. The data are for tangles with $\ell$ of about 0.14–0.16 mm. The solid lines represent power-law fits to the data in the shaded region.

by counterflow and ring injections at various $\ell$ and $T$. It is clear that $\gamma_1$ is around 1.6 nearly independent of $\ell$, which is in good agreement with the experimental observations [19]. We also see that $\gamma_1$ increases by less than 0.3 from 1.1 to 1.9 K, which is hardly resolvable in the narrow temperature range examined in the experiment. At a given $T$, the $\gamma_1$ value for tangles produced by counterflow is slightly larger than that for random tangles produced by ring injections. This difference becomes more visible as $T$ increases. Interestingly, it has been known that the vortex tangle produced by counterflow becomes increasingly anisotropic as $T$ increases [20]. This tangle anisotropy could be the origin of the observed difference, which is a topic for future research.

*Discussion.*—The weak temperature dependence of $\gamma_1$ indeed reflects interesting physics. To explain it, we show in Fig. 5 the normalized $C_x(t')/C_x(0)$ curves for vortex tangles produced by counterflow at various $T$ with $\ell$ in the range of 0.14–0.16 mm. The curve for a random tangle produced by ring injections at 0 K with $\ell = 0.16$ mm is also included as a reference. Compared to the $T = 0$ curve, a major difference of the curves at finite $T$ is that they saturate to 1 at larger $t'$. This saturation, which corresponds to ballistic motion of the vortices [i.e., $\langle \Delta x^2(t) \rangle \propto t^2$ according to Eq. (2)], is controlled by how the turbulent energy decays. At 0 K, the turbulent energy can cascade to scales smaller than $\ell$ by exciting Kelvin waves on the vortices [47]. These waves result in small-scale deformations of the vortices, which can cause rapid directional change of the vortex velocity [30] and hence suppress the velocity temporal correlation. As such, $C_x(t')$ at 0 K remains far from saturation down to $t' = 10^{-3}$ s. At finite $T$, the mutual friction from the normal fluid damps out the Kelvin waves and terminates the energy cascade at scales comparable to $\ell$ [48,49], which results in smoother vortices. Therefore, the vortices can maintain their ballistic motion to larger $t'$. The extension of the ballistic region first makes the $C_x(t')/C_x(0)$ curve steeper in the power-law region, leading to a larger exponent $\beta$ as compared to the 0 K case. As $T$ further increases, the power-law region gradually shrinks and levels off, which reduces $\beta$. The decrease in $\beta$ then causes $\gamma_1$ to gradually rise as observed in Fig. 4.

Y. T. and W. G. are supported by the National Science Foundation under Grant No. DMR-2100790 and the U.S. Department of Energy under Award No. DE-SC0020113. They also acknowledge the support and resources provided by the National High Magnetic Field Laboratory at Florida State University, which is supported by the National Science Foundation Cooperative Agreement No. DMR-1644779 and the state of Florida. S. Y. is supported by the Grant-in-Aid for JSPS Fellow program under Grant No. JP19J00967. M. T. acknowledges the support by the JSPS KAKENHI program under Grant No. JP20H01855. H. K. acknowledges the support by the JSPS KAKENHI program under Grant No. JP22H01403.

*These authors contributed equally to this work.
†wguo@magnet.fsu.edu
‡hkobayas@keio.jp
§tsubota@osaka-cu.ac.jp

[1] Y. Feng and M. Krumholz, Early turbulent mixing as the origin of chemical homogeneity in open star clusters, Nature (London) **513**, 523 (2014).
[2] C. C. Wang, K. A. Prather, J. Sznitman, J. L. Jimenez, S. S. Lakdawala, Z. Tufekci, and L. C. Marr, Airborne transmission of respiratory viruses, Science **373**, eabd9149 (2021).
[3] K. R. Sreenivasan, Turbulent mixing: A perspective, Proc. Natl. Acad. Sci. U.S.A. **116**, 18175 (2019).
[4] W. F. Vinen and J. J. Niemela, Quantum turbulence, J. Low Temp. Phys. **128**, 167 (2002).
[5] D. R. Tilley and J. Tilley, *Superfluidity and Superconductivity*, 3rd ed. (Institute of Physics, Bristol, 1990).
[6] J. Koplik and H. Levine, Vortex Reconnection in Superfluid Helium, Phys. Rev. Lett. **71**, 1375 (1993).
[7] G. E. Volovik, Classical and quantum regimes of superfluid turbulence, JETP Lett. **78**, 533 (2003).
[8] P. Walmsley, D. Zmeev, F. Pakpour, and A. Golov, Dynamics of quantum turbulence of different spectra, Proc. Natl. Acad. Sci. U.S.A. **111**, 4691 (2014).
[9] A. W. Baggaley, J. Laurie, and C. F. Barenghi, Vortex-Density Fluctuations, Energy Spectra, and Vortical Regions in Superfluid Turbulence, Phys. Rev. Lett. **109**, 205304 (2012).
[10] Y. Tang, S. Bao, T. Kanai, and W. Guo, Statistical properties of homogeneous and isotropic turbulence in He II measured via particle tracking velocimetry, Phys. Rev. Fluids **5**, 084602 (2020).
[11] Y. Tang, W. Guo, V. S. L'vov, and A. Pomyalov, Eulerian and Lagrangian second-order statistics of superfluid $^4$He grid turbulence, Phys. Rev. B **103**, 144506 (2021).

[12] P. M. Walmsley and A. I. Golov, Quantum and Quasiclassical Types of Superfluid Turbulence, Phys. Rev. Lett. **100**, 245301 (2008).

[13] L. F. Gomez *et al.*, Shapes and vorticities of superfluid helium nanodroplets, Science **345**, 906 (2014).

[14] G. P. Bewley, D. P. Lathrop, and K. R. Sreenivasan, Superfluid helium: Visualization of quantized vortices, Nature (London) **441**, 588 (2006).

[15] D. E. Zmeev, F. Pakpour, P. M. Walmsley, A. I. Golov, W. Guo, D. N. McKinsey, G. G. Ihas, P. V. E. McClintock, S. N. Fisher, and W. F. Vinen, Excimers $he_2^*$ as Tracers of Quantum Turbulence in $^4$He in the $t = 0$ Limit, Phys. Rev. Lett. **110**, 175303 (2013).

[16] B. Mastracci and W. Guo, Characterizing vortex tangle properties in steady-state He II counterflow using particle tracking velocimetry, Phys. Rev. Fluids **4**, 023301 (2019).

[17] M. Tsubota, T. Araki, and W. F. Vinen, Diffusion of an inhomogeneous vortex tangle, Physica (Amsterdam) **329B–333B**, 224 (2003).

[18] E. Rickinson, N. G. Parker, A. W. Baggaley, and C. F. Barenghi, Inviscid diffusion of vorticity in low-temperature superfluid helium, Phys. Rev. B **99**, 224501 (2019).

[19] Y. Tang, S. Bao, and W. Guo, Superdiffusion of quantized vortices uncovering scaling laws in quantum turbulence, Proc. Natl. Acad. Sci. U.S.A. **118**, e2021957118 (2021).

[20] H. Adachi, S. Fujiyama, and M. Tsubota, Steady-state counterflow quantum turbulence: Simulation of vortex filaments using the full Biot-Savart law, Phys. Rev. B **81**, 104511 (2010).

[21] W. F. Vinen, Mutual friction in a heat current in liquid helium II. I. Experiments on steady heat currents, Proc. R. Soc. A **240**, 114 (1957).

[22] J. Gao, W. Guo, V. S. L'vov, A. Pomyalov, L. Skrbek, E. Varga, and W. F. Vinen, Decay of counterflow turbulence in superfluid $^4$He, JETP Lett. **103**, 648 (2016).

[23] H. Takeuchi, S. Ishino, and M. Tsubota, Binary Quantum Turbulence Arising from Countersuperflow Instability in Two-Component Bose-Einstein Condensates, Phys. Rev. Lett. **105**, 205301 (2010).

[24] G. Greenstein, Superfluid turbulence in neutron stars, Nature (London) **227**, 791 (1970).

[25] B. Haskell, D. Antonopoulou, and C. F. Barenghi, Turbulent, pinned superfluids in neutron stars and pulsar glitch recoveries, Mon. Not. R. Astron. Soc. **499**, 161 (2020).

[26] W. H. Zurek, Cosmological experiments in superfluid-helium?, Nature (London) **317**, 505 (1985).

[27] G. W. Stagg, N. G. Parker, and C. F. Barenghi, Ultraquantum turbulence in a quenched homogeneous Bose gas, Phys. Rev. A **94**, 053632 (2016).

[28] L. D. Landau and E. M. Lifshitz, *Fluid Mechanics*, 2nd ed. (Pergamon Press, Oxford, 1987), Vol. 6.

[29] K. W. Schwarz, Three-dimensional vortex dynamics in superfluid $^4$He: Homogeneous superfluid turbulence, Phys. Rev. B **38**, 2398 (1988).

[30] M. Tsubota, T. Araki, and S. K. Nemirovskii, Dynamics of vortex tangle without mutual friction in superfluid $^4$He, Phys. Rev. B **62**, 11751 (2000).

[31] See Supplemental Material at http://link.aps.org/supplemental/10.1103/PhysRevLett.129.025301 for videos and further discussions of the numerical method.

[32] W. H. Press, B. P. Flannery, S. A. Teukolsky, and W. T. Vetterling, *Numerical Recipes in C. The Art of Scientific Computing* (Cambridge University Press, Cambridge, England, 1992).

[33] A. C. White, C. F. Barenghi, N. P. Proukakis, A. J. Youd, and D. H. Wacks, Nonclassical Velocity Statistics in a Turbulent Atomic Bose-Einstein Condensate, Phys. Rev. Lett. **104**, 075301 (2010).

[34] H. Adachi and M. Tsubota, Numerical study of velocity statistics in steady counterflow quantum turbulence, Phys. Rev. B **83**, 132503 (2011).

[35] A. W. Baggaley, The sensitivity of the vortex filament method to different reconnection models, J. Low Temp. Phys. **168**, 18 (2012).

[36] D. Ben-Avraham and S. Havlin, *Diffusion and Reactions in Fractals and Disordered Systems* (Cambridge University Press, Cambridge, England, 2000).

[37] Y. Sagi, M. Brook, I. Almog, and N. Davidson, Observation of Anomalous Diffusion and Fractional Self-Similarity in One Dimension, Phys. Rev. Lett. **108**, 093002 (2012).

[38] T. H. Harris, E. J. Banigan, D. A. Christian, C. Konradt, E. D. Tait Wojno, K. Norose, E. H. Wilson, B. John, W. Weninger, A. D. Luster *et al.*, Generalized Lévy walks and the role of chemokines in migration of effector CD8+ T cells, Nature (London) **486**, 545 (2012).

[39] V. Zaburdaev, S. Denisov, and J. Klafter, Lévy walks, Rev. Mod. Phys. **87**, 483–530 (2015).

[40] J. P. Bouchaud and A. Georges, Anomalous diffusion in disordered media: Statistical mechanisms, models and physical applications, Phys. Rep. **195**, 127 (1990).

[41] M. S. Paoletti, M. E. Fisher, K. R. Sreenivasan, and D. P. Lathrop, Velocity Statistics Distinguish Quantum Turbulence from Classical Turbulence, Phys. Rev. Lett. **101**, 154501 (2008).

[42] A. C. Davison and D. R. Cox, Some simple properties of sums of randoms variable having long-range dependence, Proc. R. Soc. A **424**, 255 (1989).

[43] I. M. Mazzitelli and D. Lohse, Lagrangian statistics for fluid particles and bubbles in turbulence, New J. Phys. **6**, 203 (2004).

[44] W. F. Vinen, Mutual friction in a heat current in liquid helium II. III. Theory of the mutual friction, Proc. R. Soc. A **242**, 493 (1957).

[45] R. J. Donnelly, *Quantized Vortices in Helium II* (Cambridge University Press, Cambridge, England, 1991), Vol. 2.

[46] R. J. Donnelly and C. F. Barenghi, The observed properties of liquid helium at the saturated vapor pressure, J. Phys. Chem. Ref. Data **27**, 1217 (1998).

[47] D. Kivotides, J. C. Vassilicos, D. C. Samuels, and C. F. Barenghi, Kelvin Waves Cascade in Superfluid Turbulence, Phys. Rev. Lett. **86**, 3080 (2001).

[48] J. Gao, W. Guo, and W. F. Vinen, Determination of the effective kinematic viscosity for the decay of quasiclassical turbulence in superfluid $^4$He, Phys. Rev. B **94**, 094502 (2016).

[49] J. Gao, W. Guo, S. Yui, M. Tsubota, and W. F. Vinen, Dissipation in quantum turbulence in superfluid $^4$He above 1 K, Phys. Rev. B **97**, 184518 (2018).